Summary: The polylactide-based nano-composites were prepared via melt extrusion method using different types of intercalants and nano-fillers having different surface charge density. In order to understand the direct polymer melt intercalation into the nano-galleries, the interdigitated layer structure of the organically modified layered filler (OMLF), where the intercalants are oriented with some inclination to the host layer in the interlayer space, was proposed. After polymer melt intercalation, the smaller initial interlayer opening led to the larger interlayer expansion, suggesting the large amount of the intercalation of the polymer chains. Consequently, the nano-composite exhibited finer dispersion of the nano-fillers when compared with the nano-composites prepared from OMLFs with larger initial interlayer opening.

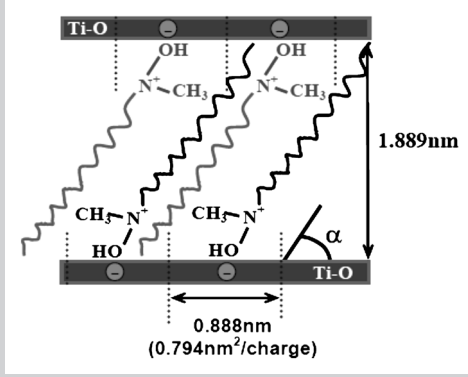

Illustration of a model of interlayer structure of the $qC_{14}(OH)$ in gallery space of HTO.

Direct Melt Intercalation of Polylactide Chains into Nano-Galleries: Interlayer Expansion and Nano-Composite Structure

*Osamu Yoshida, Masami Okamoto**

Advanced Polymeric Nanostructured Materials Engineering, Graduate School of Engineering, Toyota Technological Institute, Hisakata 2-12-1, Tempaku, Nagoya 468-8511, Japan
E-mail: okamoto@toyota-ti.ac.jp

Received: February 3, 2006; Revised: March 7, 2006; Accepted: March 14, 2006; DOI: 10.1002/marc.200600080

Keywords: chain; intercalation; interdigitated layer structure; nano-composites; polylactide; surface charge density

Introduction

Continued progress in nano-scale controlling as well as an improved understanding of the physicochemical phenomena at the nano-galleries of the layered silicates, have contributed to the rapid development of polymer/layered silicate nano-composites.[1] To the best of our knowledge, however, the direct melt intercalation kinetics in the nano-composite formation are not very well explored in literatures.

In the preceding paper,[2] we reported that an optimal interlayer structure on organically modified layered filler (OMLF) is most favorable for nano-composite formation with respect to the number per area and size of surfactant chains. In the study, we presented the interdigitated layer structure model of the OMLF, where the intercalants are oriented with some inclination to the host layer in the interlayer space. In this paper, in order to prove the importance of the interdigitated layer structure in the direct melt intercalation, we report the melt intercalation of polylactide chains into the nano-galleries based on OMLFs having different types of intercalants and nano-fillers with different charge density.

Experimental Part

A commercial poly(L-lactide) (PLA) with a *D* content of 1.1–1.7% ($\bar{M}_w = 1.87 \times 10^5$, $\bar{M}_w/\bar{M}_n = 1.76$, $T_g \approx 60\,^{\circ}C$, and $T_m \approx 168\,^{\circ}C$) supplied by Unitika Co. Ltd., Japan was dried under vacuum at 60 °C and kept under dry nitrogen gas for one week prior to use. The molecular weight and thermal properties were determined by gel permeation chromatography and differential scanning calorimeter, respectively.[3]

The various types of OMLFs having different types of intercalants and different fillers used in this study, were synthesized by replacing Na^+ ions in different nano-fillers with

Table 1. Characteristic parameters of nano-fillers.

Parameters	HTO	*syn*-FH	MMT
Chemical formula	$H_{1.07}Ti_{1.73}O_{3.95}0.5H_2O$	$Na_{0.66}Mg_{2.6}Si_4O_{10}(F)_2$	$Na_{0.33}(Al_{1.67}Mg_{0.33})Si_4O_{10}(OH)_2$
Particle size, nm	≈100–200	≈100–200	≈100–200
BET area, $m^2 \cdot g^{-1}$	≈2 400	≈800	≈700
CEC[a], meq per 100 g	≈200 (660)	≈120 (170)	≈90 (90)
e^-, charge $\cdot nm^{-2}$	1.26	0.971	0.708
Density, $g \cdot cm^{-3}$	2.40	2.50	2.50
Refractive index (n_D^{20})	2.3	1.55	1.55
pH	4–6	9–11	7.5–10

[a] Methylene blue adsorption method. The values in the parenthesis are calculated from chemical formula of nano-fillers.

alkylammonium cations (i.e., octadecylammonium, octadecyl trimethylammonium, dioctadecyl dimethylammonium, and *N*-(cocoalkyl)-*N*,*N*-[bis(2-hydroxyethyl)]-*N*-methyl ammonium cations).[4,5] The layer titanate (HTO) is a new nano-filler having high-surface charge density[4] compared with conventional layered silicates. Their names, chemical formula, and designations (as written in the text) are presented in Table 1.

The details of the nano-composites preparation were described in our previous papers.[4,5] The nano-structure analyses of wide-angle X-ray diffraction (WAXD) and transmission electron microscopy (TEM) were carried out using the same apparatus as in the previous articles.[3–5] Here we briefly describe molecular modeling of the intercalants. By aid of computer simulation, we proposed the molecular dimensions of two different intercalants using the molecular dynamics program (MM2 in Quantum CAChe, Fujitsu Ltd.) in consideration of van der Waals radi. Optimization of structure is based on minimization of the total energy of the molecular system. Molecular simulation represents a very powerful tool in the material science, but it is meaningful only in combination with experimental methods.

Results and Discussion

Characterization of Nano-Fillers

In characterizing layered silicate including layered titanate (HTO), the surface charge density is particularly important because it determines the interlayer structure of intercalants as well as cation exchange capacity (CEC). G. Lagaly proposed the method consisting of total elemental analysis and the dimension of the unit cell:[6]

$$\text{Surface charge}: \ e^- \cdot nm^{-2} = \xi/ab \qquad (1)$$

where ξ is the layer charge (1.07 for HTO, 0.66 for synthetic fluorine hectrite (*syn*-FH) and 0.33 for montmorillonite (MMT). a and b are cell parameters of HTO ($a = 3.782$ Å, $b = 2.978$ Å[7]), *syn*-FH ($a = 5.24$ Å, $b = 9.08$ Å[8]), and MMT ($a = 5.18$ Å, $b = 9.00$ Å[6]). For *syn*-FH, however, about 30% of the interlayer Na^+ ions are not replaced quantitatively by intercalants due to the non-active for ion-exchange reactions.[8] For HTO, only 27% of interlayer H^+ (H_3O^+) is active for ion-exchange reactions.[4] The remaining part is the non-active sites in the HTO. Thus, the incomplete replacement of the interlayer ions is ascribed to the intrinsic chemical reactivity. The characteristic parameters of two nano-fillers are also summarized in Table 1. HTO has high-surface charge density of 1.26 $e^- \cdot nm^{-2}$ compared with those of *syn*-FH (0.971 $e^- \cdot nm^{-2}$) and MMT (0.780 $e^- \cdot nm^{-2}$). From these results, we can estimate the average distance between exchange sites, which is calculated to be 0.888 nm for HTO, 1.014 nm for *syn*-FH, and 1.188 nm for MMT, respectively. This estimation assumes that the cations are evenly distributed in a cubic array over the silicate surface and that half of the cations are located on the one side of the platelet and the other half reside on the other side.

Molecular Dimensions and Interlayer Structure

The calculated models of the intercalant structures are presented in Figure 1. For octadecylammonium ($C_{18}H_3N^+$), obtained molecular length, thickness, and width are 2.466, 0.301, and 0.301 nm, respectively. Since the length of all alkyl units are more than 2 nm, these spacings (distance between exchange sites) of 0.888–1.188 nm do not allow parallel layer arrangement like flat-lying chains[6] in each gallery space of the nano-fillers. The all intercalants are oriented with some inclination to the host layer in the interlayer space to form an interdigitated layer. This is suggested by paraffin-type layer structure proposed by G. Lagaly, especially in case of high-surface-charged clay minerals.[6]

Wide-angle X-ray diffraction patterns for three OMLF powders are presented in Figure 2. The mean interlayer spacing of the (001) plane [$d_{(001)}$] for the HTO intercalated with $qC_{14}(OH)$ [HTO-$qC_{14}(OH)$] obtained by WAXD measurements is 2.264 nm (diffraction angle, $2\Theta \cong 3.90^\circ$). The appearances of small peaks observed at $2\Theta \cong 7.78^\circ$, 11.78°, and 15.74° were confirmed that these reflections were due to (002) up to (004) plane of HTO-$qC_{14}(OH)$. HTO-$qC_{14}(OH)$ surprisingly well-ordered suprastructure proved by WAXD with diffraction maxima

(a) octadecylammonium [$C_{18}H_3N^+$]

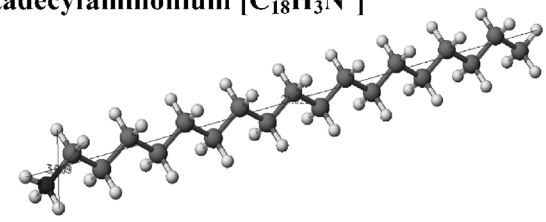

(b) octadecyltrimethylammonium [$C_{18}(CH_3)_3N^+$]

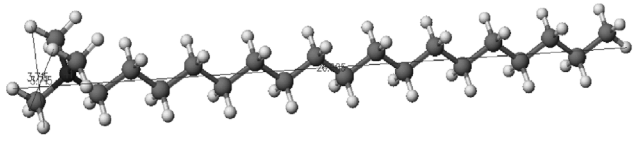

(c) dioctadecyldimethylammonium [$2C_{18}(CH_3)_2N^+$]

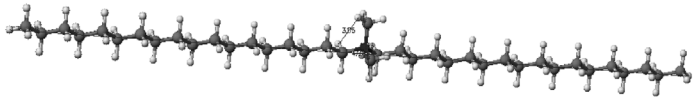

(d) *N*-(cocoalkyl)-*N*,*N*-[bis(2-hydroxyethyl)]-*N*-methyl ammonium [$qC_{14}(OH)$]

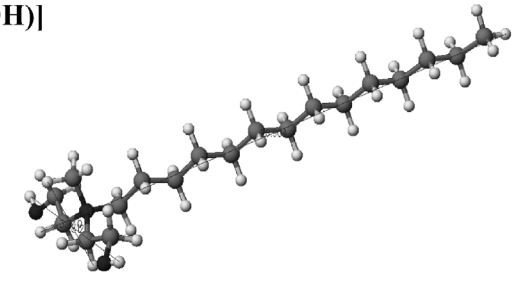

Intercalant	$C_{18}H_3N^+$	$C_{18}(CH_3)_3N^+$	$2C_{18}(CH_3)_2N^+$	$qC_{14}(OH)$
Length /nm	2.466	2.601	4.766	2.090
Thickness /nm	0.301	0.372	0.434	0.374
Width /nm	0.301	0.372	0.318	0.881

Figure 1. Molecular dimensions of intercalants: (a) octadecylammonium ($C_{18}H_3N^+$); (b) octadecyltrimethylammonium [$C_{18}(CH_3)_3N^+$]; (c) dioctadecyldimethylammonium [$2C_{18}(CH_3)_2N^+$]; and (d) *N*-(cocoalkyl)-*N*,*N*-[bis(2-hydroxyethyl)]-*N*-methyl ammonium cations [$qC_{14}(OH)$].

up to the fourth order due to the high-surface charge density of the HTO layers. On the other hand, *syn*-FH and MMT, which have low-surface charge density compared with that of HTO, show less-ordered interlayer structure. That is, the coherent order of the silicate layers is much lower in each *syn*-FH and MMT intercalated with surfactants.

From WAXD results, we can discuss the interlayer opening that is estimated after subtraction of the layer thickness value of 0.374 nm for HTO,[7] 0.98 nm for *syn*-FH,[8] and 0.96 nm for MMT.[6] This is an important point for the following discussion on the interlayer structure. The illustration of a model of interlayer structure of the $qC_{14}(OH)$ in gallery space of the HTO is shown in Figure 3. For nano-fillers with high-surface charge density, the intercalants can adopt a configuration with orientation where the alkyl chains are tilted under the effect of the van der Waals forces, which decreases the chain-chain distance. For this reason, the angle α should be directly related to the packing density of the alkyl chains. The value of α decreases until close contact between the chains is attained, giving an increase of the degree of the crystallinity of the intercalants into the nano-galleries. To estimate the tilt angle α, we combined the molecular dimension, interlayer spacing, and loading amount of intercalant in the layers, which was

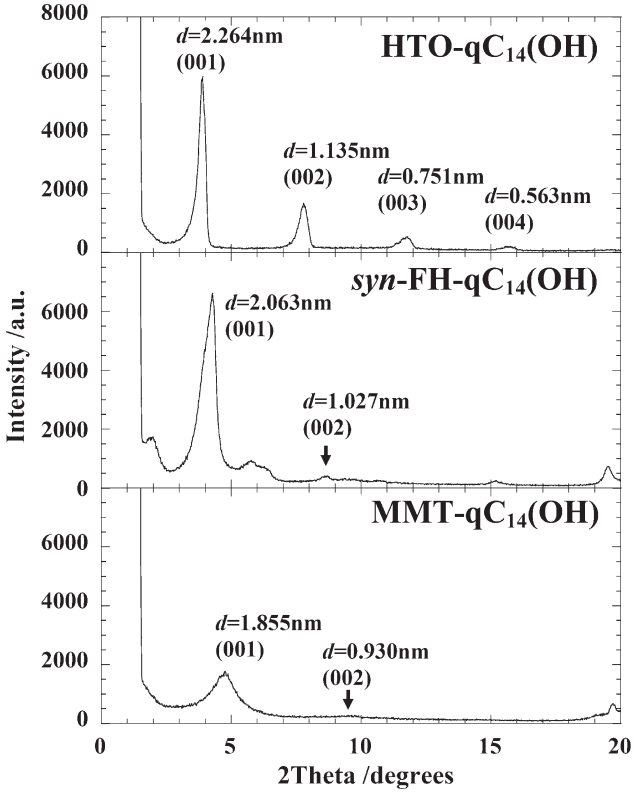

Figure 2. WAXD patterns of (a) HTO, (b) *syn*-FH, and (c) MMT intercalated with $qC_{14}(OH)^+$.

calculated from thermogravimetry analysis (TGA). The characteristic parameters are summarized in Table 2 and 3. Note that HTO exhibits large value of layer opening accompanied with large values of α and endothermic heat flow ΔH due to the melting of the intercalants in the galleries when compared with those of *syn*-FH and MMT. This indicates that HTO leads to a high-interdigitated layer structure and the interlayer opening becomes more uniform compared with MMT and *syn*-FH (possessing lower surface charge density).

From to this fact, we can observe well-defined diffraction peaks up to (004) plane (see Figure 2). The entropic contribution of the intercalants, which leads to the entropy gain associated with the layer expansion after intercalation of the polymer chains, may not be significant because of the interdigitated layer structure.

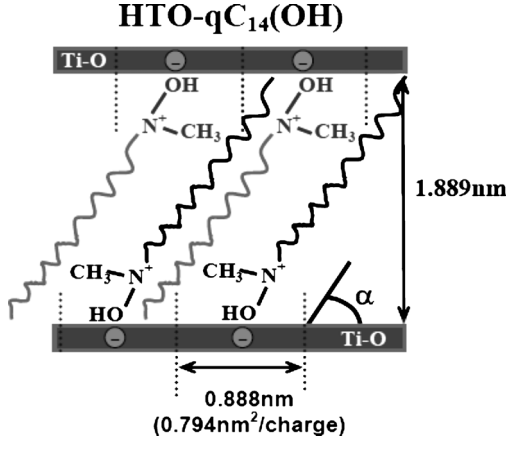

Figure 3. Illustration of a model of interlayer structure of the $qC_{14}(OH)$ in gallery space of HTO.

Correlation of Intercalant Structure and Interlayer Opening

For the interdigitated layer structure in MMT, alkyl chain length, i.e., $C_{18}H_{37}$, CH_3, and $(CH_2)_2OH$ in the amine structure, changes the interlayer opening. That is, when we compare different intercalants having same long alkyl chain [i.e., $C_{18}H_3N^+$ and $C_{18}(CH_3)_3N^+$], three methyl (CH_3) substituents instead of hydrogen (H) disturb the contact with silicate surfaces. The value of α decreases until close contact between the ammonium cations and silicate surfaces is attained, giving a decreasing of the interlayer opening [$d_{(001)}$] (see Table 3 and Figure 2).

In case of intercalant having two long alkyl chains [i.e., $2C_{18}(CH_3)_2N^+$], the packing density of the alkyl chains is reduced and sterically limited into the nano-galleries. Consequently, MMT-$2C_{18}(CH_3)_2N^+$ exhibits large interlayer opening accompanied with low crystallinity of the intercalant ($\Delta H \approx 130\ J \cdot g^{-1}$) compared with MMT-$C_{18}H_3N^+$ and MMT-$C_{18}(CH_3)_3N^+$. Accordingly, we observed disordered diffraction peak of (001) plane of MMT-$2C_{18}(CH_3)_2N^+$ in the WAXD analysis (see Figure 1 in ref.[9]). We have to pay attention to the molecular size of the substituents instead of H attached to the nitrogen for the better understanding of the interdigitated layer structure and direct polymer melt intercalation. This feature has been observed in the results of OMLFs intercalated with various intercalants (such as octadecyl di-methylbenzylammonium, *n*-hexadecyl tri-*n*-butyl phosphonium, and *n*-hexadecyl triphenyl phosphonium cations).[10]

Nano-Composite Structure

Figure 4 shows the results of TEM bright field images of PLA-based nano-composites, in which dark entities are the cross section of intercalated MMT layers. The organically modified MMT content in all nano-composites was 4 wt.-%. From the TEM images, it becomes clear that there are some intercalated and stacked silicate layers in the nano-composites. We estimate the form factors obtained from TEM images, i.e., average value of the particle length (L), of the dispersed particles and the correlation length (ξ) between them.[7] From the WAXD patterns, the crystallite size (D) of intercalated-stacked silicate layers of each nano-composite is calculated by using Scherrer equation.[11] The calculated value of D ($\cong$ thickness of the dispersed

Table 2. Comparison of characteristic parameters among HTO, *syn*-FH, and MMT prepared with $qC_{14}(OH)$.

	HTO-$qC_{14}(OH)$	*syn*-FH-$qC_{14}(OH)$	MMT-$qC_{14}(OH)$
Layer opening, nm	1.889	1.083	0.895
Tilt angle α, °	64.4	31.1	25.3
Organic content, wt.-%	39.6	30.4	32.5
T_m [a], °C	108.3	111.3	97.7
ΔH [a], $J \cdot g^{-1}$	214.5	141.2	138.6

[a] The melting and heat flow of $qC_{14}(OH)^+Cl^-$ are 35.8 °C and 69.8 $J \cdot g^{-1}$, respectively.

particles) and other parameters for each nano-composite are presented in Table 4.

For PLA/MMT-$C_{18}(CH_3)_3N^+$, L and D are in the range of (200 ± 25) and 10.7 nm. On the other hand, PLA/MMT-$C_{18}H_3N^+$ exhibits large value of L $(450 \pm 200$ nm) with large level of stacking of the silicate layers ($D \approx 21$ nm). ξ value of the PLA/MMT-$C_{18}(CH_3)_3N^+$ $(80 \pm 20$ nm) is lower than the value of PLA/MMT-$C_{18}H_3N^+$ $(260 \pm 140$ nm), suggesting that the intercalated layers are more homogeneously and finely dispersed in case of PLA/MMT-$C_{18}(CH_3)_3N^+$. The number of the stacked individual silicate layers $[\equiv D/d_{(001)} + 1]$ is 5 for PLA/MMT-$C_{18}(CH_3)_3N^+$ and ξ value of this nano-composite is one order of magnitude lower compared with those of PLA/MMT-$C_{18}H_3N^+$ and PLA/MMT-$2C_{18}(CH_3)_2N^+$, suggesting that intercalanted silicate layers are more homogeneously and finely dispersed.

Although the (initial) interlayer opening of MMT-$C_{18}(CH_3)_3N^+$ at 1.011 nm is smaller than MMT-$C_{18}H_3N^+$ at 1.350 nm and MMT-$2C_{18}(CH_3)_2N^+$ at 1.540 nm, the intercalation of the PLA in these different OMLFs gives almost same basal spacing after preparation of the nano-composites. Note that the existence of sharp Bragg peak in PLA-based nano-composites after melt extrusion clearly indicates that the dispersed silicate layers still retain an ordered structure after melt extrusion.

In Table 4, we summarized the layer expansion after preparation (Δ opening) of three nano-composites, or after subtraction of the initial layer opening. For same MMT with different intercalants [e.g., comparison between MMT-$C_{18}(CH_3)_3N^+$ and MMT-$2C_{18}(CH_3)_2N^+$], the layer expansion of the former (0.879 nm) exhibits large value compared with that of the later (0.45 nm) in PLA-based nano-composites. In other words, the smaller interlayer opening caused by the configuration with small tilt angle [$\alpha = 22.9°$ for $C_{18}(CH_3)_3N^+$] promotes the large amount of the intercalation of the polymer chains. Accordingly, PLA/MMT-$C_{18}(CH_3)_3N^+$ exhibits finer dispersion of the nano-fillers compared with PLA/MMT-$2C_{18}(CH_3)_2N^+$ and PLA/MMT-$C_{18}H_3N^+$ as discussed before (see Figure 4).

Table 3. Comparison of characteristic parameters of MMT-based OMLF prepared with $C_{18}H_3N^+$, $C_{18}(CH_3)_3N^+$, and $2C_{18}(CH_3)_2N^+$.

	$C_{18}H_3N^+$	$C_{18}(CH_3)_3N^+$	$2C_{18}(CH_3)_2N^+$
Layer opening, nm	1.350	1.011	1.540
Tilt angle α, °	33.2	22.9	40.1
Organic content, wt.-%	35.5	29.5	39.8
T_m [a], °C	69.9	69.5	44.0
ΔH [a], $J \cdot g^{-1}$	177.7	189.6	129.7

[a] The meltings and heat flows of $C_{18}H_3N^+$ Cl^-, $C_{18}(CH_3)_3N^+$ Cl^-, and $2C_{18}(CH_3)_2N^+$ Cl^- are 83.8 °C and 95.6 $J \cdot g^{-1}$; 103.5 °C and 161.2 $J \cdot g^{-1}$; 37.0 °C and 54.6 $J \cdot g^{-1}$, respectively.

One more interesting feature is the absolute value of Δ opening. According to the molecular modeling, the width and thickness of the PLA are 0.76 and 0.58 nm. This may suggest that the polymer chains could not penetrate into galleries in case of MMT-$2C_{18}(CH_3)_2N^+$ when we compare the apparent interlayer expansion (Δ opening).

Now it is necessary to understand the meaning of the interlayer expansion in the intercalated nano-composites. As discussed before, we have to take the interdigitated layer structure into consideration. This structure may suggest that the different orientation angle could adopt when the polymer chains penetrate into the galleries, giving a decreasing of the basal spacing after intercalation. At the same time, this structure apparently provides a balance between the polymer penetration and different orientation angle of the intercalants. That is, we have to pay attention to the polymer chains intercalation into the galleries from the result of the change of the basal spacing as revealed by WAXD. Presumably the penetration of the polymer chain is prevented or reduced by the steric-limitation of the configuration with large value of α (e.g., $\alpha = 40.1°$ for MMT-$2C_{18}(CH_3)_2N^+$). Accordingly, we sometimes observe small interlayer expansion and encounter a decreasing of the interlayer spacing after melt intercalation. As seen in Table 4, the initial interlayer opening depends on the interlayer expansion (Δ opening) after melt intercalation. The smaller initial opening leads to the larger interlayer expansion, and gives almost same final interlayer opening. This feature has been observed in the results of other nano-composites prepared by different OMLFs intercalated with different surfactants.[12] As reported in our previous paper,[2] the pressure drop (Δp) into the

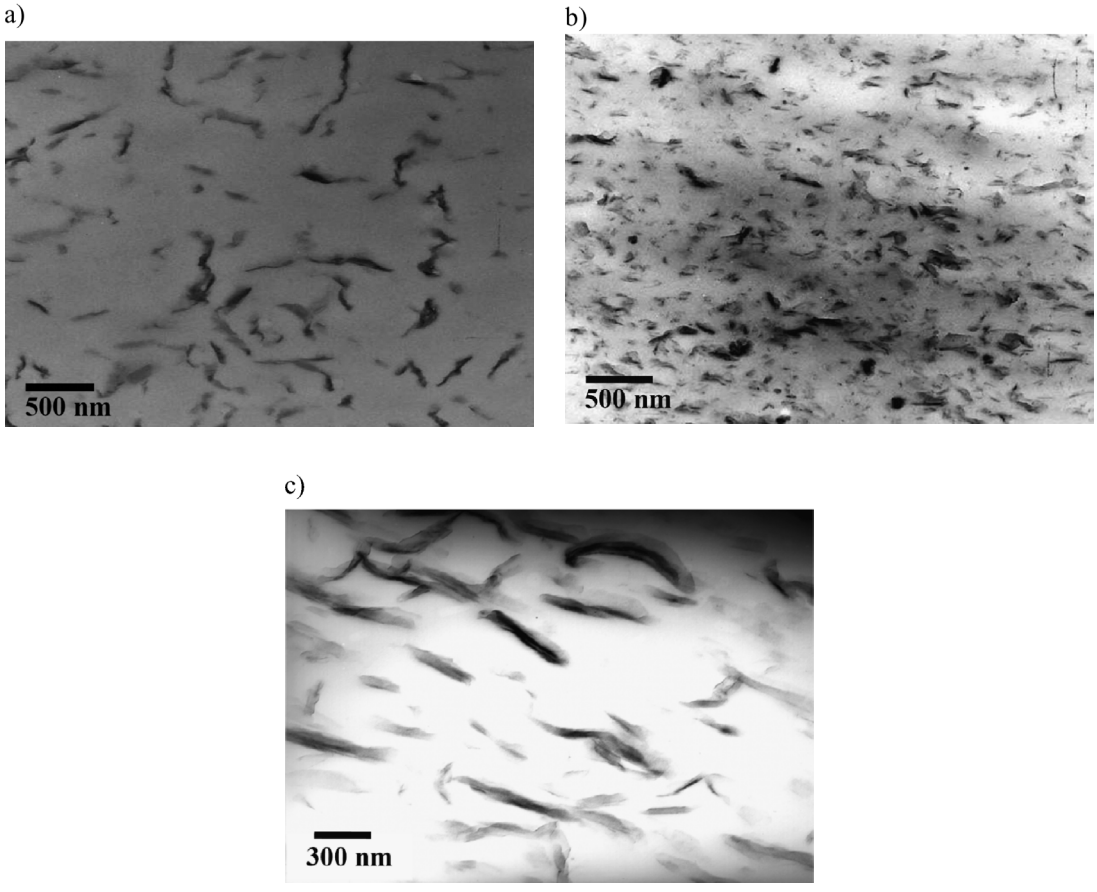

Figure 4. Bright filed TEM images of PLA-based nano-composites prepared with (a) MMT-$C_{18}H_3N^+$, (b) MMT-$C_{18}(CH_3)_3N^+$, and (c) MMT-$2C_{18}(CH_3)_2N^+$. The dark entities are the cross section and/or face of intercalated and stacked silicate layers and the bright areas are the matrix.

nano-galleries, which makes the polymer penetration more difficult, should be discussed. The estimated pressure difference (24 MPa) is much larger than the shear stress (0.1 MPa) during melt compounding.[2]

This suggests that shear stress has little effect on the delamination (exfoliation) of the layer. This reasoning is consistent with the intercalated structure reported by so many nano-composite researchers, who can prepare only intercalated (not exfoliated) nano-composites via simple melt extrusion technique.[13] A novel compounding process is currently in progress and we will report it separately.

Conclusion

In this study, we proposed the interdigitated layer structure of the OMLFs, where the intercalants are oriented with some inclination to the host layer in the interlayer space. Owing to the high-surface charge density, HTO provides to well-ordered interdigitated layer structure and the interlayer opening becomes more uniform compared with *syn*-FH- and MMT-based nano-fillers.

For the better understanding of PLA chains melt intercalation into the nano-galleries, we have to take the interdigitated layer structure into consideration. This

Table 4. Form factors of three nano-composites obtained from WAXD and TEM observations.

Nano-composites	PLA/MMT-$C_{18}H_3N^+$	PLA/MMT-$C_{18}(CH_3)_3N^+$	PLA/MMT-$2C_{18}(CH_3)_2N^+$
d_{001}, nm	3.03	2.85	2.95
Δ opening, nm	0.72	0.879	0.45
Final layer opening, nm	2.07	1.89	1.99
D, nm	20.9	10.73	14.71
$(D/d_{001})+1$	7.9	4.8	6.0
L, nm	450 ± 200	200 ± 25	655 ± 121
ξ, nm	260 ± 140	80 ± 20	300 ± 52

structure suggests that the different orientation angle can adopt when the polymer chains penetrate into the galleries. After polymer melt intercalation, the smaller interlayer opening caused by the configuration with small tilt angle promotes the large amount of the intercalation of the PLA chains. Accordingly, PLA/MMT-$C_{18}(CH_3)_3N^+$ exhibits finer dispersion of the nano-fillers compared with PLA/MMT-$2C_{18}(CH_3)_2N^+$ and PLA/MMT-$C_{18}H_3N^+$ as revealed by TEM images.

[1] M. Okamoto, "Recent Advances in Polymer/Layer Silicate Nanocomposites: An Overview from Science to Technology", in: *Advances in Processing and Properties of Polymer Nanocomposites*, S. G. Advani, Ed., World Scientific, Singapore 2006 (in press).
[2] O. Yoshida, M. Okamoto, *J. Polym. Eng.* **2006** (in press).
[3] S. Sinha Ray, P. Maiti, M. Okamoto, K. Yamada, K. Ueda, *Macromolecules* **2002**, *35*, 3104.
[4] R. Hiroi, S. Sinha Ray, M. Okamoto, T. Shiroi, *Macromol. Rapid Commun.* **2004**, *25*, 1359.
[5] S. Sinha Ray, K. Yamada, M. Okamoto, A. Ogami, K. Ueda, *Chem. Mater.* **2003**, *15*, 1456.
[6] G. Lagaly, *Clay Miner.* **1970**, *16*, 1.
[7] S. Nakano, T. Sasaki, K. Takemura, M. Watanabe, *Chem. Mater.* **1998**, *10*, 2044.
[8] H. Tateyama, S. Nishimura, K. Tsunematsu, K. Jinnai, Y. Adachi, M. Kimura, *Clays Clay Miner.* **1992**, *40*, 180.
[9] S. Sinha Ray, K. Yamada, M. Okamoto, K. Ueda, *J. Nanosci. Nanotech.* **2003**, *3*, 503.
[10] O. Yoshida, T. Saito, M. Okamoto, in preparation.
[11] S. Sinha Ray, K. Yamada, M. Okamoto, K. Ueda, *Polymer* **2003**, *44*, 857.
[12] O. Yoshida, T. Saito, M. Okamoto, in preparation.
[13] S. Sinha Ray, M. Okamoto, *Prog. Polym. Sci.* **2003**, *28*, 1539.